

## Electrical Detection of Spin Pumping due to the Precessing Magnetization of a Single Ferromagnet

M. V. Costache, M. Sladkov, S. M. Watts, C. H. van der Wal, and B. J. van Wees

*Physics of Nanodevices Group, Materials Science Centre, University of Groningen,  
Nijenborgh 4, 9747 AG Groningen, The Netherlands*

(Received 1 September 2006; published 22 November 2006)

We report direct electrical detection of spin pumping, using a lateral normal-metal/ferromagnet/normal-metal device, where a single ferromagnet in ferromagnetic resonance pumps spin-polarized electrons into the normal metal, resulting in spin accumulation. The resulting backflow of spin current into the ferromagnet generates a dc voltage due to the spin-dependent conductivities of the ferromagnet. By comparing different contact materials (Al and/or Pt), we find, in agreement with theory, that the spin-related properties of the normal metal dictate the magnitude of the dc voltage.

DOI: 10.1103/PhysRevLett.97.216603

PACS numbers: 72.25.Ba, 72.25.Hg

Recent theoretical work in the field of spintronics [1–3] proposes to realize nanodevices in which a so-called spin-pumping mechanism is used for polarizing electron spins in a normal-metal (paramagnetic) region. Spin pumping [1] is a mechanism where a pure spin current is emitted at the interface between a ferromagnet with a precessing magnetization and a normal-metal region. It is an important new mechanism for controlling spins, since other electronic methods based on driving an electrical current through a ferromagnet ( $F$ )–normal-metal ( $N$ ) interface [4] are strongly limited by the so-called conductance mismatch [5]. Until now, however, spin pumping has been demonstrated only with thin multilayers, where it appears as an enhanced damping of magnetization dynamics in ferromagnetic resonance experiments [6–9].

In this Letter, we present spin pumping with a single nanomagnet in an electronic device, in which it is directly detected as a dc electronic signal. This opens up new ways to detect magnetization dynamics on a nanoscale. The elementary mechanism is based on the parametric spin pumping proposed in Ref. [1]. As shown in Fig. 1(c), a spin current  $\mathbf{I}_s^{\text{pump}} = (1/4\pi)\hbar g_{\perp} \mathbf{m} \times d\mathbf{m}/dt$  is pumped by (resonant) precession of a ferromagnet magnetization into an adjacent normal-metal region.  $\mathbf{m}$  is the magnetization direction, and  $g_{\perp}$  is the mixing conductance [10], a material parameter which describes spin transport perpendicular to  $\mathbf{m}$  at the interface. Depending on the spin-related properties of the normal metal, two regimes exist. When the normal metal is a good “spin sink” (in which spins relax fast), the injected spin current is dissipated fast, and this corresponds to a loss of angular momentum and an increase in the effective Gilbert damping of the magnetization precession [6–9]. However, in the limit of the spin flip relaxation rate smaller than the spin injection rate, a spin angular momentum builds up in the normal metal; i.e., a spin accumulation  $\mu_S$  (the difference between the chemical potentials for spins up and down) exists in the normal metal close to the interface [2]. Because of electron diffusion in the normal metal, the spin accumulation can diffuse

away from the interface and, in principle, can be measured electrically by using a second ferromagnet as a spin-dependent contact, placed at a distance shorter than the spin flip length [2,11].

However, Wang *et al.* [3] predicted a more direct way to detect it by converting the spin accumulation into a voltage using the precessing ferromagnet as its own detector, as illustrated in Fig. 1(c). As a result of  $\mu_S$ , a backflow current goes back into  $F$ . The component parallel to  $\mathbf{m}$  can enter  $F$  and gives rise to a dc voltage due to the spin-dependent conductivities (bulk and interface) of the ferromagnet. Therefore, in a device geometry where a ferromagnet is contacted with two normal-metal electrodes, any asymme-

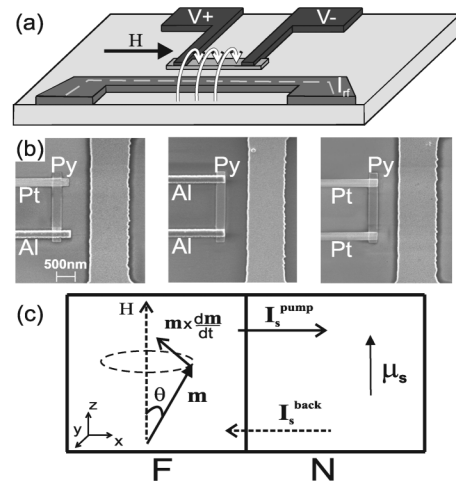


FIG. 1. (a) Schematic diagram of the device. On the lower side, through the shorted end of a coplanar strip, a current  $I_{\text{rf}}$  generates an rf magnetic field, denote by the arrows. The Py strip in the center produces a dc voltage  $\Delta V = V^+ - V^-$ .  $H$  denotes the static magnetic field applied along the strip. (b) Scanning electron microscope pictures of the central part of the devices. (c) The  $F/N$  structure in which the resonant precession of the magnetization direction  $\mathbf{m}$  pumps a spin current  $\mathbf{I}_s^{\text{pump}}$  into  $N$ . The spin pumping builds up a spin accumulation  $\mu_S$  in  $N$  that drives a spin current  $\mathbf{I}_s^{\text{back}}$  back into  $F$ .

try between the two contacts can result in a net dc voltage. The largest such asymmetry is obtained when one of the metal electrodes is a spin sink (for which we expect negligible dc voltage) such as Pt, while the other has a small spin flip relaxation rate, such as Al. Here we describe precise, room-temperature measurements of the dc voltage across a ferromagnetic strip contacted by Pt and Al electrodes when the ferromagnet is in resonance. As control devices, we also used contact configurations consisting of two Pt electrodes and two Al electrodes. We found that the primary contribution to the observed dc voltages comes from the Al contact, thus allowing us to rule out spurious magnetoresistive contributions.

Figure 1(a) shows a schematic illustration of the lateral devices used in the present study. The central part of the device is a ferromagnetic strip of permalloy ( $\text{Ni}_{80}\text{Fe}_{20}$ , or Py) connected at both ends to normal metals, Al and/or Pt ( $V^-$  and  $V^+$  contacts). The devices are fabricated on a Si/SiO<sub>2</sub> substrate using *e*-beam lithography, material deposition, and liftoff. A 25 nm thick Py strip with  $0.3 \times 3 \mu\text{m}^2$  lateral size was *e*-beam deposited in a base pressure of  $1 \times 10^{-7}$  mBar. Prior to deposition of the 30 nm thick Al or/and Pt contact layers, the Py surface was cleaned by Ar ion milling, using an acceleration voltage of 500 V with a current of 10 mA for 30 s, removing the oxide and a few nanometers of Py material to ensure transparent contacts. We measured in total 17 devices (this includes 4 devices with a modified contact geometry, described later). Different contact material configurations are shown in Fig. 1(b).

We measured the dc voltage generated between the  $V^+$  and  $V^-$  electrodes as a function of a slowly sweeping magnetic field ( $H$ ) applied along the Py strip ( $z$  axis), while applying an rf magnetic field ( $h_{\text{rf}}$ ) perpendicular to the strip ( $y$  axis). We have recently shown [12] that a submicron Py strip can be driven into the uniform precession ferromagnetic resonance mode, using a small perpendicular rf magnetic field created with an on-chip coplanar strip waveguide [13] positioned close to the Py strip (similar geometry as shown in Fig. 1). For the used rf power level (9 dBm), an rf current of  $\approx 12$  mA [14] passes through the shorted end of the coplanar strip waveguide and creates an rf magnetic field with an amplitude of  $h_{\text{rf}} \approx 1.6$  mT at the location of the Py strip. We could confirm that on resonance the precession cone angle is  $\approx 5^\circ$  [15].

To reduce the background (amplifier) dc offset and noise, we adopted a lock-in microwave frequency modulation technique. During a measurement where the static magnetic field is swept from  $-400$  to  $+400$  mT, the rf field is periodically switched between two different frequencies, and we measured the difference in dc voltage between the two frequencies  $\Delta V = V(f_{\text{high}}) - V(f_{\text{low}})$  using a lock-in amplifier. For all of the measurements, the lock-in frequency is 17 Hz, and the difference between the two microwave frequencies is 5 GHz.

Figure 2 shows the electric potential difference  $\Delta V$  from a Pt/Py/Al device. Sweeping the static magnetic field in a range  $-400$  to  $+400$  mT, a peak and a diplike signal are

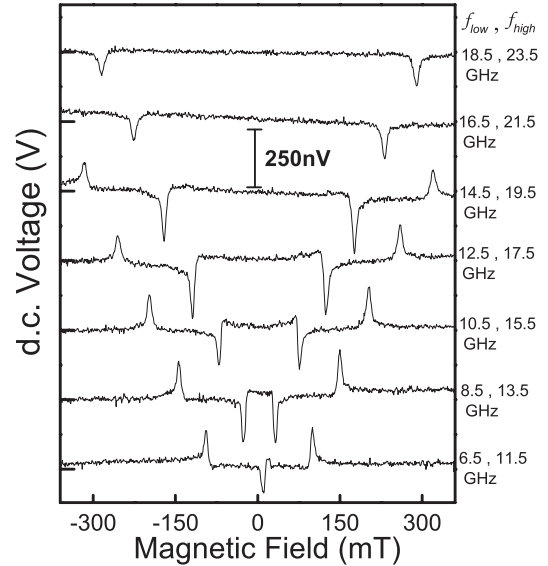


FIG. 2. The dc voltage  $\Delta V$  generated by a Pt/Py/Al device in response to the rf magnetic field plotted as a function of the static magnetic field. The frequencies of the rf field are as shown. The peaks (dips) correspond to resonance at  $f_{\text{high}}$  ( $f_{\text{low}}$ ). The data are offset vertically, for clarity.

observed at both positive and negative values of the static field. Since we measured the difference between two frequencies, the peak corresponds to the high resonant frequency ( $f_{\text{high}}$ ) and the dip to the low resonant frequency ( $f_{\text{low}}$ ). For the opposite sweep direction, the traces are nominally identical. We measured 8 devices with contact material Pt/Py/Al. The measured resonances are all in the range  $+100$  to  $+250$  nV. Notably, the dc voltages are all of the same sign (always a peak for  $f_{\text{high}}$ ), meaning that, for Pt/Py/Al devices, the Al contact at resonance is always more negative than the Pt contact.

First, we look at peak/dip position dependence of the rf frequency. In Fig. 3(a), the dc voltage in gray scale is plotted versus the static field for different high (low) frequencies of the rf field. Figure 3(b) shows the fitting of the peak/dip position dependence of the rf field frequency (dotted curve) using Kittel's equation for a small angle precession of a thin-strip ferromagnet [16]:

$$f = \frac{\gamma}{2\pi} \sqrt{(H + N_{\parallel} M_S)(H + N_{\perp} M_S)}, \quad (1)$$

where  $\gamma$  is the gyromagnetic ratio,  $N_{\parallel}$  and  $N_{\perp}$  are in-plane (along the width of the strip) and out-of-plane demagnetization factors, and  $M_S$  is the saturation magnetization. The fit to this equation [see Fig. 3(b)] gives  $\gamma = 176$  GHz/T, and  $N_{\parallel} \mu_0 M_S = 60$  mT,  $N_{\perp} \mu_0 M_S = 930$  mT, consistent with earlier reports [12,17]. The fit confirms that the dc voltage appears at the uniform ferromagnetic resonance mode of the Py strip. Second, we measured the peak/dip amplitudes for different values of the applied rf current [14] [Fig. 3(c)]. We observe here a linear dependence on

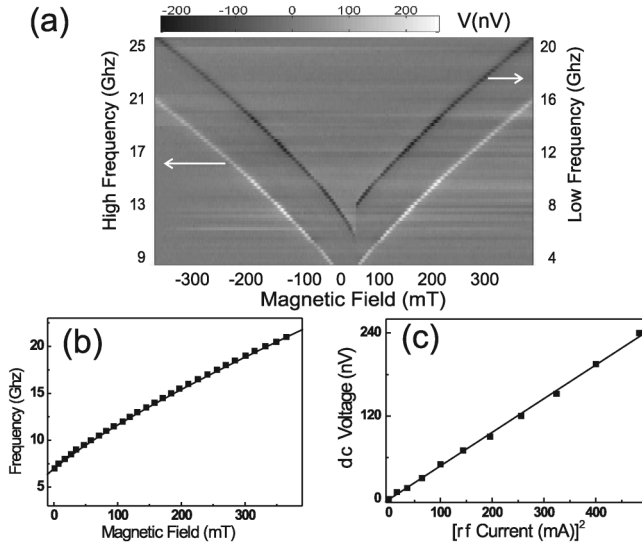


FIG. 3. (a) Gray scale plot of the dc voltage  $\Delta V$ , a measured function of static field for different high (low) frequencies of the rf field from the Pt/Py/Al device [21]. The dark (light) curves denote resonance at  $f_{\text{low}}$  ( $f_{\text{high}}$ ). (b) The static magnetic field dependence of the resonance frequency of the Py strip (dots). The curve is a fit to Eq. (1). (c) The amplitude of the dc voltage from a Al/Py/Al device as a function of the square of the rf current, at 13 GHz and 139 mT (dots). The line shows a linear fit.

the square of the rf current. This is consistent with the prediction of the spin-pumping theory, as explained below.

Further, we studied several control devices where the Py strip is contacted at both ends by the same nonmagnetic material Al (5 devices) or Pt (4 devices). Here we expected no signal because: (i) symmetry reasons—the voltages for identical interfaces are the same (but opposite) and their contribution to  $\Delta V$  cancels. (ii) Pt has a very short spin diffusion length, resulting in a small spin accumulation, a small backflow, and thus a lower signal. The results from Al/Py/Al devices show smaller signals than Pt/Py/Al devices, with a large scatter in amplitude and both with positive and negative sign for the resonance at  $f_{\text{high}}$ . Typical values for the 5 devices are  $-100$  [shown in Fig. 4(a)],  $+25$ ,  $+30$ ,  $+75$ , and  $+110$  nV. In contrast, all 4 Pt/Py/Pt devices exhibit only weak signals up to 20 nV [with resonance signals barely visible, as in Fig. 4(b)]. We attribute the signals from Al/Py/Al devices to the asymmetry of the two contacts [possibly caused by a small variation in the contact geometry and interface; see Fig. 1(b)]. Depending on the asymmetry, the signal therefore has a scatter around zero. In the Pt/Py/Pt devices, independent of possible asymmetry, we expected and found very small signals. We therefore conclude that the resonances measured with the Pt/Py/Al devices arises mainly from the Al/Py interface (the Pt/Py/Al devices have signals that are always positive, on average  $\approx +150$  nV, and with a scatter comparable in amplitude to that of Al/Py/Al devices around zero).

In order to obtain the magnetization precession cone angle  $\theta$  [15], we performed anisotropic magnetoresistance

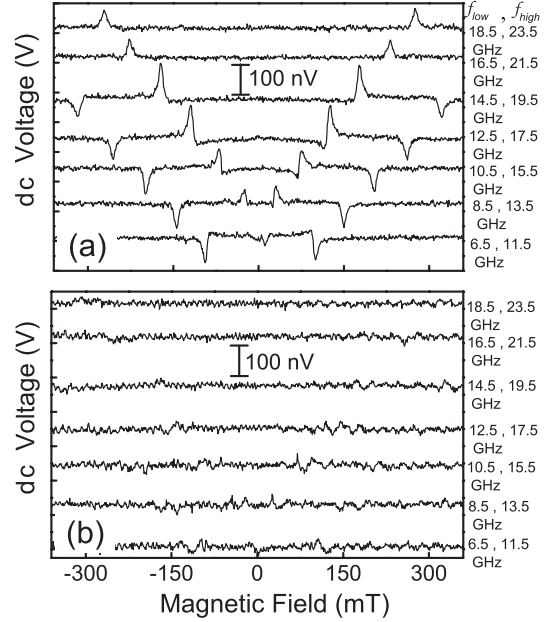


FIG. 4. The dc voltage  $\Delta V$  generated across the (a) Al/Py/Al and (b) Pt/Py/Pt devices as a function of the static magnetic field. The frequencies of the rf field are as shown.

(AMR) measurements. The measurements were carried out as before (at 15.5 GHz), but in addition a dc current (typically  $50 \mu\text{A}$ ) was sent through the Py strip. Around the ferromagnetic resonance, an extra signal due to the AMR effect is measured (that is linear with the applied dc current). For the AMR effect, the change in the resistance ( $V/I$ ) of the Py depends on the angle between the dc current and the (time-averaged) direction of the magnetization as  $R(\theta) = R_0 + \Delta R_{\text{AMR}} \cos^2(\theta)$ , where  $R_0$  is the resistance of the strip when the magnetization is perpendicular on the direction of the current and  $\Delta R_{\text{AMR}}$  is the change in the resistance between the parallel and perpendicular directions of the magnetization. From the amplitude of the dc-current-induced contribution to the resonance, and using a measured AMR value of 2% for our Py strip, we obtained  $\theta$  to be  $\approx 5^\circ$ . This value is consistent with the value  $\theta \approx h_{\text{rf}}/(\alpha M_S) = 6^\circ$  calculated using the solution of the linearized Landau-Lifshitz-Gilbert equations. Here a damping parameter of  $\alpha = 0.01$  results from fitting the AMR voltage shape at resonance with the frequency-dependent value of  $\theta^2$  [15].

We also checked that the observed resonances do not arise from rectification effects that can result from time-dependent AMR. We analyzed [15] that due to the capacitive and inductive coupling between the coplanar strip waveguide and the Py strip an rf current can be induced in the detection circuit. In combination with a time-dependent AMR (which can contain a component with rf frequency  $\omega$ ), this can lead to a rectification effect where a dc voltage is created. To rule out a possible contribution to the measured resonance signals, we have studied 4 devices similar to Fig. 1(b), but now with contacts at the ends of the

Py strip (extending along the  $\mathbf{z}$  axis) [18]. We found no significant difference in the observed dc voltages between this geometry and that shown in Fig. 1(b). Further, we misaligned the direction of the static field with respect to the Py strip long axis and only found significant contributions from rectification effects at offset angles higher than  $5^\circ$ . This rules out that small offset angles caused significant effects in the present study.

We now analyze the results. As can be seen in Fig. 1(c), due to a time-dependent magnetization direction  $\mathbf{m}$ , the pumped spin current has a constant component in the  $\mathbf{z}$  direction and oscillating components in the  $\mathbf{x}$  and  $\mathbf{y}$  directions. Here we are interested in the description for small  $\theta$ . We do not take into account spin relaxation in  $N$  because for small  $\theta$  the spin relaxation in  $F$  will be the dominant mechanism for controlling the magnitude of the dc voltage. The dynamics of  $\mathbf{x}$  and  $\mathbf{y}$  components of spin are controlled by the length scale  $l_\omega = \sqrt{D_N/\omega}$  ( $D_N$  is the diffusion coefficient in  $N$ , and  $\omega$  is the precessional frequency) which describes the length scale over which the averaging of  $\mathbf{x}$  and  $\mathbf{y}$  components occurs. In our experiment,  $l_\omega$  of Al is of the order of 200–300 nm. This means that, in principle, we have to fully model spin dynamics in this region. However, we follow Wang *et al.* to get a qualitative estimate of the effect. It is assumed that  $\mathbf{x}$ ,  $\mathbf{y}$  components are fully averaged and, therefore, zero, and the remaining  $\mathbf{z}$  component is constant and along the static magnetic field direction [2]. Also, for small  $\theta$ , the component of spin accumulation  $\mu_S$  parallel to  $\mathbf{m}$  is approximately equal to  $\mu_S$ . This component can diffuse back into  $F$  and give rise to a dc voltage due to spin-dependent conductivities. Thus, a voltage of  $p_\omega \mu_S$  will be generated across the interface. For a small angle precession, this results in [3]

$$V_{\text{dc}} = \frac{p_\omega g_\omega^\parallel}{2e(1 - p_\omega^2)g_\omega} \theta^2 \hbar \omega, \quad (2)$$

where  $p_\omega = (g_\omega^\uparrow - g_\omega^\downarrow)/(g_\omega^\uparrow + g_\omega^\downarrow)$  and  $g_\omega = g_\omega^\uparrow + g_\omega^\downarrow$ , with  $g_\omega^\uparrow$  ( $g_\omega^\downarrow$ ) the spin-up (-down) effective conductances of the Py/Al interface [19]. The quadratic dependence of  $V_{\text{dc}}$  on  $\theta$  in Eq. (2) is in agreement with the experimental data [see Fig. 3(c)]. Having determined a precession cone angle  $\theta \approx 5^\circ$ , using  $p_\omega \approx 0.2$ , a ferromagnetic resonance frequency  $\omega = 10^{11} \text{ s}^{-1}$ , and  $g_\omega^\parallel/g_\omega \approx 1$ , we find  $V_{\text{dc}} \approx 100 \text{ nV}$ , in agreement with the experimental results.

In summary, we have measured a dc voltage due to the spin-pumping effect, across the interface between Al and Py at ferromagnetic resonance. We find that the devices where the Al contact has been replaced by Pt show a voltage close to zero, in good agreement with theory. Although the prediction of the spin-pumping model agrees with the observed dc voltage values, a more detailed description is required that would include the elliptical precession motion of the ferromagnet's magnetization as well as the spin dynamics in  $N$  [20]. These results demonstrate

the feasibility of directly converting magnetization dynamics of a single nanomagnet into an electrical signal.

We thank X. Wang and G. E. W. Bauer for discussion. This research was supported by the Dutch Organization for Fundamental Research on Matter (FOM).

- 
- [1] Y. Tserkovnyak, A. Brataas, and G. E. W. Bauer, *Phys. Rev. Lett.* **88**, 117601 (2002).
  - [2] A. Brataas, Y. Tserkovnyak, G. E. W. Bauer, and B. I. Halperin, *Phys. Rev. B* **66**, 060404(R) (2002).
  - [3] X. Wang, G. E. W. Bauer, B. J. van Wees, A. Brataas, and Y. Tserkovnyak, preceding Letter, *Phys. Rev. Lett.* **97**, 216602 (2006).
  - [4] F. J. Jedema, A. T. Filip, and B. J. van Wees, *Nature (London)* **410**, 345 (2001).
  - [5] G. Schmidt, D. Ferrand, L. W. Molenkamp, A. T. Filip, and B. J. van Wees, *Phys. Rev. B* **62**, R4790 (2000).
  - [6] S. Mizukami, Y. Ando, and T. Miyazaki, *J. Magn. Magn. Mater.* **226**, 1640 (2001); *Phys. Rev. B* **66**, 104413 (2002).
  - [7] R. Urban, G. Woltersdorf, and B. Heinrich, *Phys. Rev. Lett.* **87**, 217204 (2001).
  - [8] B. Heinrich, Y. Tserkovnyak, G. Woltersdorf, A. Brataas, R. Urban, and G. E. W. Bauer, *Phys. Rev. Lett.* **90**, 187601 (2003).
  - [9] K. Lenz, T. Tolinski, J. Lindner, E. Kosubek, and K. Baberschke, *Phys. Rev. B* **69**, 144422 (2004).
  - [10] A. Brataas, Y. V. Nazarov, and G. E. W. Bauer, *Phys. Rev. Lett.* **84**, 2481 (2000).
  - [11] F. J. Jedema, H. B. Heersche, A. T. Filip, J. J. A. Baselmans, and B. J. van Wees, *Nature (London)* **416**, 713 (2002); F. J. Jedema, M. V. Costache, H. B. Heersche, J. J. A. Baselmans, and B. J. van Wees, *Appl. Phys. Lett.* **81**, 5162 (2002).
  - [12] M. V. Costache, M. Sladkov, C. H. van der Wal, and B. J. van Wees, *Appl. Phys. Lett.* **89**, 192506 (2006).
  - [13] K. C. Gupta, R. Garg, I. Bahl, and P. Bhartia, *Microstrip Lines and Slotlines* (Artech House, Inc., Norwood, MA, 1996).
  - [14] The 9 dBm applied rf power was converted into a rf current assuming 50 load impedance.
  - [15] M. V. Costache, S. M. Watts, M. Sladkov, C. H. van del Wal, and B. J. van Wees, *Appl. Phys. Lett.* (to be published).
  - [16] C. Kittel, *Introduction to Solid State Physics* (Wiley, New York, 1996), 7th ed., Chap. 16.
  - [17] F. Giesen, J. Podbielski, T. Korn, M. Steiner, A. van Staa, and D. Grundler, *Appl. Phys. Lett.* **86**, 112510 (2005).
  - [18] In this geometry, the induced rf current flows through the contacts predominantly parallel to the magnetization direction. This suppresses a possible contribution to the measured dc voltages from a rectification effect at the contacts [15].
  - [19]  $g_\omega^\uparrow$  ( $g_\omega^\downarrow$ ) are the spin-up (-down) interface conductances in series with a conductance of the bulk normal metal over a length scale of  $l_\omega$ , and  $g_\omega^\parallel$  is the mixing conductance evaluated over a length scale of  $l_\omega$ .
  - [20] X. Wang, G. E. W. Bauer, A. Brataas, and Y. Tserkovnyak (unpublished).
  - [21] The irregular feature, occurring only near  $H = 0 \text{ mT}$ , is due to magnetization switching with hysteresis.